SPE 140468-PP

An Alternative Interpretation of Microseismic Events during Hydraulic Fracturing

Arash Dahi Taleghani, Juan M. Lorenzo, Louisiana State University

This paper was prepared for presentation at the SPE Hydraulic Fracturing Technology Conference and Exhibition held in The Woodlands, Texas, USA, 24–26 January 2011.

Abstract

It is common practice in industry to monitor hydraulic fracturing jobs by picking major, micro-earthquake events in seismograms whose source locations form a spatial pattern used for interpreting induced fractures. Surprisingly, controversy still surrounds the interpretation of these scattered, discrete events. Many authors conclude that hydraulic fractures are generated by shear failure events rather than tensile failures. This interpretation contradicts our common understanding of fracture mechanics, which describes the hydraulic fracture process as taking place predominantly in mode-I failure (pure tension). We propose that band-width limited instrumentation during seismic field recording may be partly to blame. Low-frequency (<5 Hz) tensile-source events which are expected to occur continuously between shear events are largely ignored. Herein, we try to compare the total energy of detected shear events with the total energy of expected low-frequency tensile events in the background in order to justify the main (tensile) mechanism of fracturing. Major, shear-mechanism events may not describe accurately the temporal and spatial pattern of induced fractures in the subsurface. Shear events may only represent the locations where hydraulic fractures intersect pre-existing discontinuities. Therefore, by only considering shear events, we may not be able to make a correct estimation of the orientation and extension of the hydraulic fractures. We suggest that only by recording silent (low frequency) events, we will truly be able to describe induced subsurface fracture geometries.

Introduction

During the last decade, hydraulic fracturing has become a popular procedure to enhance production in new unconventional gas resources (including shale gas). Production improvement depends mainly on the geometry of the induced fracture. Owing to limited access of the subsurface, direct observation of induced fractures is almost impossible. Therefore, different methods have been proposed in the literature to estimate the size of fractures. Among these methods, pressure analysis (Smith 1993) and microseismic monitoring (Meadows and Winterstein, 1994) have attracted most attention.

Hydraulic fractures induce two large changes as they are progress through a reservoir. The stress in the surrounding rock (especially in the tip vicinity) is perturbed because of fracture opening, and consequently pore pressure also increases as a result of leakoff and higher stresses. Both these changes may generate elastic waves, which are similar to silent or small earthquakes, called microseisms. Microseisms can be detected by sensitive geophones in nearby wells. The compressional waves (P-waves) and shear waves (S-waves) of microseisms travel at different speeds. So, if a receiver can detect both P- and S-waves from a single point source microseism, the time separation can be used to determine distance of the single event providing that the velocity field between the source and the receiver is known sufficiently, barring the effects of noise, anisotropy and heterogeneity (Eisner et al., 2009). The direction in space can be determined using triaxial receivers and/or array rotation to examine the polarization of the P-wave.

More energetic fractures (higher rate, larger volume or higher net pressure) are expected to result in more microseismic

energy release. However, various field data show that the minimum magnitude of the detected microseism event in geophones increases with offset as a result of attenuation of small signals of weak events with distance (Warpinski, 2010). For this reason, sensors are placed at close offsets in wells rather than at surface locations.

Currently, one major concern in the technology is the proper location and extent of tension fractures induced by fluid pressuring. Stricter environmental regulations may hinder shale gas industrial development in the future in the US. The United States Environmental Protection Agency (EPA) is currently reviewing the potential hazard of fluids, used during hydraulic fracturing, to contaminate the environment. Fracturing fluid may contain kerosene, benzene, toluene, xylene, and formaldehyde. These chemicals are not directly used as treating chemical additives but can be a small component of the specific chemicals used in the job and a small dosage of these chemical could very poisonous to humans. In one case, unstable fracturing led to a blowout in another well in Clearfield County, PA on June 3, 2010. More than 35,000 gallons of hydraulic fracturing fluids were thrown into the air and on to the surrounding landscape in a forested area. Campers were evacuated and the company (EOG Resources), and the well completion company (C.C. Forbes) have been ordered to cease all operations in the state of Pennsylvania, pending investigation.

In this paper, we are trying to advance an approach which considers the frequency range for the seismic events observed during hydraulic fracturing events. Earthquake seismic waves can be interpreted by means of a well-developed method for finding the location and source mechanism of tectonic earthquakes (e.g., Aki and Richards 1991). The method for interpreting hydraulic fracturing seismic events, however, is still at a rudimentary stage because of the lack of a comprehensive physical model of its source mechanism.

There are numerous examples of fieldwork worth recorded microseismic data. The cloud of microseismic epicenters have been plotted and used to interpret fracture properties. However, several questions still remain unanswered: What origin do these microseismic events have? What is their frequency content? And does shear event provide reliable information about the fracture geometry or it could be simply due to stress changes around the wellbore? Answers to these questions will determine the share between tensile and shear failure mechanisms in the rock. Improved knowledge of the rock failure mechanism will lead to a better understanding of the fracture process and consequently enhanced hydraulic fracture designs.
Injection of fluid into subsurface geological structures, such as faults and fractures, reduces the effective normal stress acting across these structures. If sufficient shear stress is present, the structure may slip in shear and generate seismic events over a range of magnitudes. Subsidence is not directly caused by hydraulic fracturing but may occur after considerable production of oil or ground water. Subsidence occurs over reservoirs whether they have been subject to hydraulic fracturing or not because it is a result of producing fluids from the reservoir and lowering the reservoir pore pressure. The subsidence process can be associated with some seismicity. Reports of minor tremors of no greater than 2.8 on the Richter scale on June 2, 2009 in Cleburne, Texas - the first in the town's 140-year history can be interpreted based on this scenario, but in general, shear events in recorded in the other formations may only represent the large-scale heterogeneity of rock properties or the locations where hydraulic fractures intersect pre-existing discontinuities. For instance, pre-existing natural fractures in reservoirs may provide weak paths for new fractures that are offset from their original path normal to minimum horizontal stress. In these cases, hydraulic fractures convert from pure mode-I fractures to mixed-mode-I and mode-II fractures. Therefore, our study of tensile fractures should provide a better understanding of the nature of the shear events as well. However, the PIs believe that the orientation and extension of the hydraulic fractures can be extracted from tensile events more reliably. Obviously, reliable monitoring of hydraulic fractures has a significant impact on reducing economic risks for the operators while improving safety concerns.

The widespread approach in the oil and gas industry to monitor hydraulic fracturing jobs is by picking major, micro-earthquake events in seismograms whose source locations form a spatial pattern used for interpreting induced fractures. However, microseisms occur away from the fracture (Warpinski et al. 1997) and therefore it cannot give direct location of the joint generated during hydraulic fracture. Moreover, this interpretation contradicts our common understanding of the fracture mechanics, which describes the hydraulic fracture process as taking place predominantly in mode-I failure (pure tension). We propose that band-width limited instrumentation during seismic field recording may be partly to blame so that until now, low-frequency (< 5Hz) tensile-source events remain largely ignored. To support our argument, we first try to find a counter-part for hydraulic fracturing in nature: propagating dikes.

Evidence of Low Frequency Tensile Events in Nature

Observations and current knowledge in volcano seismology can provide insights into hydraulic fracturing problems. Magmatic dikes and hydraulic fractures are both fluid-driven. In the former, magma is the fracturing fluid, which upon eruption can vary in viscosity from 10^{-2} or 10^{-1} cP in fluid lava (Kilauea) to $10^{3} – 10^{5}$ cP in viscous lavas (Schminke, 2004)
A synthetic fracture fluid can have similar effective viscosities (10^{2}-10^{4} cP). In both cases, the original rock prior to cracking can be highly impermeable. Tight gas shales of the Haynesville Formation, Louisiana, USA and unaltered igneous rocks can both show permeabilities values of 10^{-4} to 10^{-3} D.

Volcanic events can be classified according to their frequency content (e.g., McNutt, 2005). Relatively lower-frequency events (1-2Hz) are correlated to extension-related, low-volume, deformation tremors (See Figure 1) associated with the jerky (Aki et al. 1977) progression of magma through subsurface cracks. These events are characterized by a weak high-frequency onset followed by a strong harmonic signal with frequency peak less than 2 Hz (Chouet 1996). Higher-frequency events from these same volcanic areas appear related to shear-earthquakes suggesting a similar character may exist in man-made hydraulic fracture stimulations (Figure 2). Bame and Fehler (1986) also recognized the similarity between volcanic events and hydraulic fracture experiments and ascribe the events as sudden openings of a channel that connect two fluid filled cracks. Classical hydraulic fracturing theory predicts the creation of a tensile opening of a cavity in response to fluid pressure whereas associated shear events can only be induced by indirectly changing the stress.

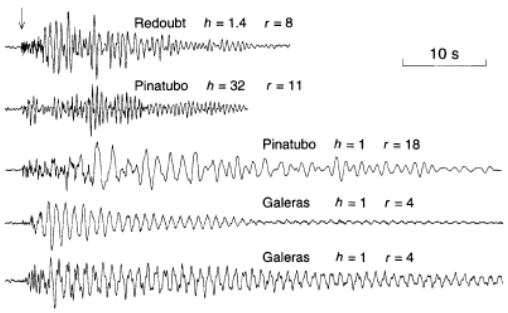

Figure 2. Typical signature of long period events observed at different volcanoes. Source depth, h, and epicentral distances, r, in km, are indicated above the seismogram of frequencies used in hydraulic fracturing monitoring (Chouet, 1996).

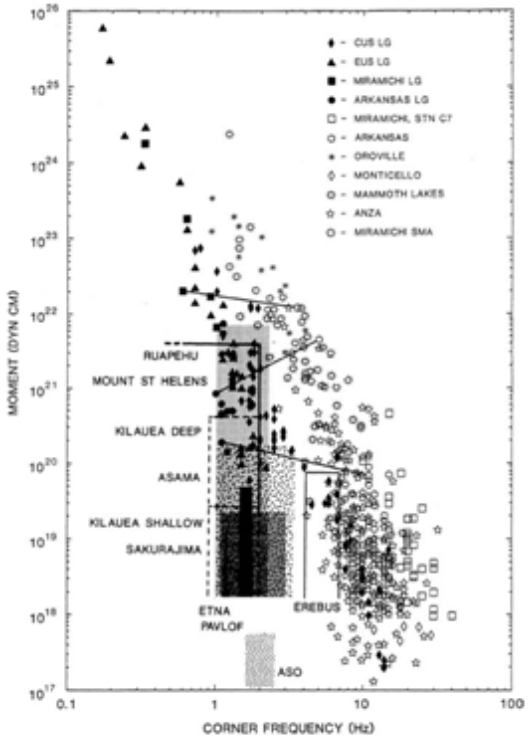

Figure 1. Various volcanic earthquakes from around the globe (McNutt, 2005) plotted according to their moment and dominant frequency conent can be separated into smaller-volume low-frequency events (shaded rectangles above) and other events mappable as faults. Lower-frequency events trend differently also imply different non-shearing mechanisms for their origin.

Many of these events have identical waveforms that represent repeated activation of a given source along fault planes. Fehler and Bame (1986) simply describe the events as sudden openings of a channel that connects two fluid-filled cracks.

Extracting more information from the seismic data requires the use of a source model, which mainly reveals the physics of the problem. For example, a double-couple source mechanism for slippage along a fault would generate very different data than a non-shearing mechanism (e.g. tensile CLVD mechanism). For this reason full moment tensor inversion procedures (Ford et al., 2009), which are used regularly in the broader seismological community (Dreger, 2000), also show great promise to improve of our understanding of hydraulic fracturing mechanisms (Figure 3). Foulger (1988) studied numerous non-double couple events with magnitudes -2 to 1 near the Hengill geothermal regions, Iceland and concluded that these events resulted from rapid tensile crack growth due to rock cooling.

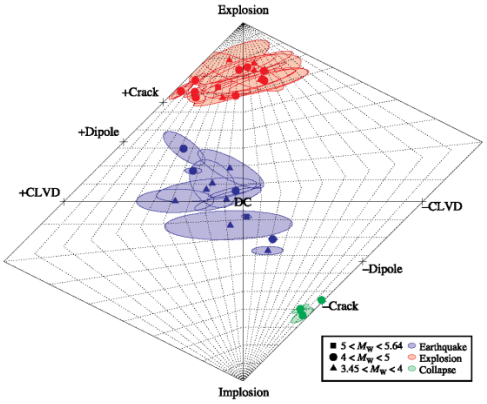

Figure 3. Source type plot shows separation of earthquakes (central confidence ellipses) and explostions (upper ellipses). Tensile cracks (+ Crack) lie along upper left edge just below identifiable explosion events (Ford, 2009).

Spectral Character of Seismograms--A Simple Analytical Fracture Propagation Model

Fracture propagation causes rock masses along the fracture to move (and also vibrate) with time. These movements generate elastic waves emitting from the growing fractures. To calculate these motions, one needs to solve elastodynamics equations for fracture growth in three-dimensional space. Although, there are bunch of analytical (Detournay, 2004; Spence and Sharp, 1985) and numerical (Adachi et al., 2007; Boone and Ingraffea, 1990; Dahi-Taleghani and Olson, 2009; Ouyang et al., 1997) techniques in literature to simulate quasi-static hydraulic fracture propagation, there is no solution for dynamic propagation of hydraulic fractures in two and three-dimensional space. The available numerical and analytical methods treat fracture propagation as quasi-static problem. It means than rather than considering a continuous variation of stress and displacement fields with time, they just consider fracture propagation in a series of snapshots. Due to complex nature of this problem even at the quasi-static level, most of the attempts so far were mainly focused on interpreting the collected field data. However as discussed before, without a good understanding of the physics of the problem and range of the frequency content of this problem, blind data processing could be futile.

On one hand a high degree of refinement in both time and space is required to accurately represent moving discontinuities associated with propagating fractures, on the other hand large domain of analysis is needed to reduce artificial interaction with the boundaries, therefore we first started by considering a semi-analytical model in an infinite elastic domain for this problem. Otherwise, reflected elastic waves could dominate the solution in the long term. For the sake of simplicity in the initial attempt to study this problem, we assumed that fluid pressure, P, is uniform along the fracture i.e. fracturing fluid has zero viscosity. This is not a realistic assumption but the proposed model has a closed-form analytical solution, so it will provide a framework for further developments to fully coupled fluid flow-rock deformation analysis.

The distribution of particle velocities on the plane strain fracture faces (one half of the fracture opening rate) at any time t is given by (Broberg, 1975; Freund, 1990):

$$\dot{u}_y(x,t) = \frac{\alpha v}{\sqrt{1-(x/vt)^2}}, \tag{1}$$

where v is the fracture propagation speed along the x axis and μ is the shear modulus of rock. The coefficient α is determined from solving the following equation

$$\frac{P}{\mu} = \alpha \frac{V_s^2}{v} \int_0^\infty \frac{R(i\xi)}{(v^{-2}+\xi^2)^{3/2}\sqrt{V_p^{-2}+\xi^2}} d\xi, \tag{2}$$

where V_p and V_s are dilatational and shear wave speed of the rock. The function $R(\eta)$ in the above equation is

$$R(\eta) = (V_s^2 - 2\eta^2)^2 + 4\eta^2\sqrt{V_p^2-\eta^2}\sqrt{V_s^2-\eta^2}. \tag{3}$$

To synthesize an example, we assumed that Young's modulus of elasticity for the rock is 30,000MPa, Poisson's ratio of 0.2 and treatment net pressure of P=4,000psi (27,579 KN/m^2). It is notable that rather than considering the fracturing fluid pressure, we considered fluid net pressure. The net pressure is the total pressure minus minimum horizontal in-situ stress, which is the driving force for fracture propagation. Equations 1-3 provide motions as well as vibrations along the fracture faces due to fracture propagation, now using the equivalent body force theorem (Burridge and Knopoff, 1964), these motions can be treated as a source for generation of seismic motions in geophones.

First, we assume that the point source geometry or a continuous distribution of point sources could be an adequate approximation to describe the seismic displacements observed from fracturing treatments. The body wave radiation from a general moment tensor M associated to a point source can be written as (Aki and Richards, 2002)

$$u_n = M_{pq} * G_{np,q}. \tag{4}$$

Based on the distance between the source and the receiver, displacement u_n can be decomposed into different components

$$u_n = u_n^N(t) + u_n^{IP}(t) + u_n^{IS}(t) + u_n^{FP}(t) + u_n^{FS}(t), \tag{5}$$

where N, I and F stand for near-field, intermediate field and far-field displacements, respectively. Intermediate-field is a misleading term as Aki and Richards (2002) states that these terms at no distance are dominant terms, however in some case (for instance Vidale et al., 1995) is shown that intermediate terms could be as effective as near-field parameters. It is possible to calculate each of these terms by solving the fundamental problem of elastodynamics.

If the charachteristic length of the fracture is assumed to be $\boldsymbol{a}$ and the distance between the source on the fracture surface to the receiver is r, then for far-field displacements, the receiver point is supposed to be far enough from the source ($r>>a$ and $r>>c/w$), which should not be confused with the point-source approximation, which assumed that $r>>a$ and $c/\omega >>a$ (ω is

the wave frequency). For sufficiently small *a* /*r*, there will a range of low frequencies where both of these inequalities are satisfied simultaneously (Rice, 1980). Typical geometries in the hydraulic fracturing problem and arrangement of microseismic geophones make far-field displacements in equation 5 the domiant terms. The far-fielddisplacements are (Shi and Ben-Zion, 2009)

$$u_n^{FP}(t) = \frac{\gamma_n \gamma_p \gamma_q}{4\rho\pi V_p^{\,3}} \frac{1}{r} \dot{M}_{pq}\left(t - \frac{r}{V_p}\right), \tag{6}$$

$$u_n^{FS}(t) = -\left(\frac{\gamma_n \gamma_p - \delta_{pn}}{4\rho\pi V_S^{\,3}}\right) \frac{1}{r} \dot{M}_{pq}\left(t - \frac{r}{V_S}\right), \tag{7}$$

where $\gamma_i = \frac{x_i}{r} = \frac{\partial r}{\partial x_i}$, $V_p = \sqrt{\frac{(\lambda + 2\mu)}{\rho}}$ and $V_S = \sqrt{\mu/\rho}$.

The moment for a displacement discontinuity, $\bar{\mathbf{u}}$ is

$$m_{pq} = \lambda \bar{u}_k \nu_k \delta_{pq} + \mu\left(\bar{u}_p \nu_q + \bar{u}_q \nu_p\right) \tag{8}$$

Accordingly, the effective moment tensor for a distributed source (here, the fracture surface) will be $M_{pq} = \int_\Sigma m_{pq} dA$. In the case of the varying displacement discontinuity, the displacements should be obtained by integrating equations (8) over the fracture or slipped area. For the special case of pure tensile dislocations, we will have $\bar{\mathbf{u}} = \Delta u_k \nu_k$,where Δu_k is the magnitude of fracture opening. Thus for a given fracture opening, moment tensor will be $m_{pq} = \lambda \Delta u_k \nu_k \delta_{pq} + \mu\left(\Delta u_k \nu_k + \Delta u_k \nu_k\right)$.

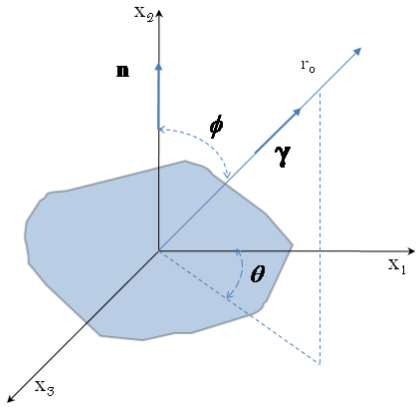

Figure 4. Planar fracture surface, and the notation used for the coordinate system.

By substituting the resultant moment tensore in equations (6-7), we will have

$$u_n^{FP}(t) = \frac{\boldsymbol{\gamma}}{4\pi r V_P}\left\{\mathbf{n}.\mathbf{v} + 2(V_S/V_P)^2(\mathbf{n}.\boldsymbol{\gamma}\,\boldsymbol{\gamma}.\mathbf{v} - \mathbf{n}.\mathbf{v})\right\}\int_A \Delta\dot{u}\left(\mathbf{x}, t - (\mathbf{r} - \boldsymbol{\gamma}.\mathbf{x})/V_P\right)dA \text{ , and} \tag{9}$$

$$u_n^{FS}(t) = -\frac{1}{4\pi r V_S}\left\{(\boldsymbol{\gamma}.\mathbf{v})\mathbf{n} + (\boldsymbol{\gamma}.\mathbf{n})\mathbf{v} - 2(\mathbf{n}.\boldsymbol{\gamma}\,\boldsymbol{\gamma}.\mathbf{v})\boldsymbol{\gamma}\right\}\int_A \Delta\dot{u}\left(\mathbf{x}, t - (\mathbf{r} - \boldsymbol{\gamma}.\mathbf{x})/V_S\right)dA \text{ ,} \tag{10}$$

where **n** is the unit vector normal to the fracture surface.

γ is the unit vector from the source center to the observer (shown in Figure 4), which can be rewritten in the spherical coordinate system as

$$\gamma_1 = \sin\phi\cos\theta, \qquad \gamma_2 = \cos\phi, \qquad \gamma_3 = \sin\phi\sin\theta. \tag{11}$$

For a tensile opening, we will have $\mathbf{v} = \mathbf{n}$; i.e. $\mathbf{v}$ is in the x_2-direction. The far-field and intermediate field displacements (Eq. 9-10) can be simplified as

$$u_n^{FP}(t) = \frac{\gamma}{4\pi r V_P}\left(1 - 2\left(V_S^{\,2}/V_P^{\,2}\right)\sin^2\phi\right)\int_A \Delta\dot{u}\left(\mathbf{x}, t - (\mathbf{r} - \boldsymbol{\gamma}.\mathbf{x})/V_P\right)dA \text{ , and} \tag{12}$$

$$u_n^{FS}(t) = -\frac{\lambda}{4\pi r V_S}\sin 2\phi \int_A \Delta\dot{u}\left(\mathbf{x}, t - (\mathbf{r} - \boldsymbol{\gamma}.\mathbf{x})/V_S\right)dA \text{ ,} \tag{13}$$

where

$$\lambda = -\frac{n - \gamma\cos\phi}{\sin\phi}.$$

By integrating equations 12-13 over the fracture surface of height h, we will have:

$$u_n^{FP}(t) = \frac{\gamma}{4\pi r V_P}\left(1 - 2\left(V_S^{\,2}/V_P^{\,2}\right)\sin^2\phi\right)h\left|\Delta\dot{u}\left(\omega\cos\gamma/V_P, \omega\right)\right| \text{, and} \tag{14}$$

$$u_n^{FS}(t) = -\frac{\lambda}{4\pi r V_S}\sin 2\phi\left|\Delta\dot{u}\left(\omega\cos\gamma/V_S, \omega\right)\right|. \tag{15}$$

By looking at the above equations, it is evident that $\Delta\dot{u}$ should be determined before using the above equations. The coupled hydraulic fracturing problem should be solved to be able to calculate the displacement discontinuities or their rates.

Therefore, if we plot $\Delta\dot{u}(\mathrm{k}, \omega)$ in *k*-ω diagram (Aki et al., 1977), we can look at far-field spectra of fracturing seismic events for all directions in a graph. Figure 5 shows such a density-plot for the analytical fracture solution given in equations 1-3. There is a surprising feature in this graph: the existence of several spectral peaks which are located at low frequencies.

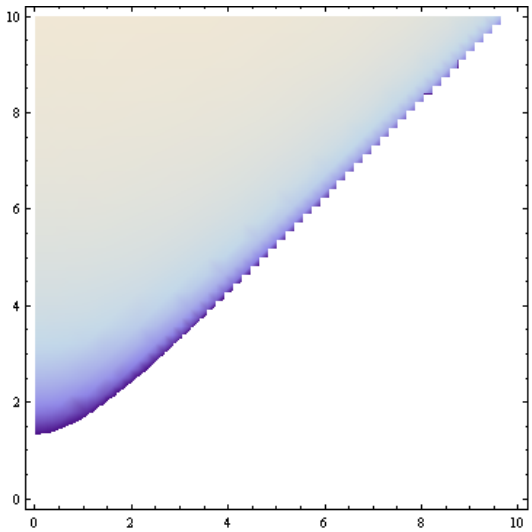

Figure 5. Plot of analytical double-Fourier transform of velocity at the source (Wave-number vs. frequency).

Coupled Hydraulic Fracturing Model (Quasi-static Case)

To calculate seismograms, we need to have the fracture opening rate profile, $\Delta\dot{w}(s,t)$ (Aki et al, 1977). However, Aki et al. (1977) only considered the microseismic event generate due to the rock deformation at the fracture tip and ignored the rock deformation due to extension/deformation in the rest of the fracture. The complete profile of fracture opening rate can be attained by solving the rock deformation and fracture fluid flow equations simultaneously. In this section, the equations governing hydraulic fractures propagation will be presented for two-dimensional geometry. This is not necessarily the most appropriate assumption for many hydraulic fracturing situations, but the presented model is a preliminary model testing an

entirely new method, and for computational simplicity, we have chosen to sacrifice the three dimensional aspects of the problem. A more complete model must ultimately add those three dimensional aspects back in the calculation. Here, we only consider small linear elastic deformations which are most appropriate in hard rock situations, but the same procedure can be developed for soft rocks by including plasticity in the fracture growth model. Stress analysis is done in plane strain geometry. The strong form of the initial boundary value problem for the fractures has the following form (Moës et al., 1999):

$$\sigma_{ij,j} + b_i = 0, \tag{16}$$

where σ is the Cauchy stress tensor, b is the body force per unit volume. The stress and strain are related by the linear elastic constitutive law as

$$\sigma_{ij} = C_{ijkl}\varepsilon_{kl}, \tag{17}$$

where C_{ijkl} are the components of the elasticity tensor. For the sake of simplicity, it is assumed that fractures are propagating in an isotropic, impermeable, linear elastic medium under plane strain conditions, and that the fracture is driven by an incompressible Newtonian fluid from a source located somewhere along the fracture (i.e. the wellbore).

Crack propagation is always assumed to be quasi-static. Given that fluid is injected into the fracture at a constant volumetric rate, Q_0, the goal is to determine the fracture length as a function of time, and the fracture opening as a function of time t and position (x,y). The aspect ratio of fractures, width to the length, is typically less than 10^{-3}, which is to say that hydraulically induced fractures are long and thin. An almost similar ratio is expected to fracture height to the length ration. The long thin geometry of the fluid flow, together with the high viscosity of the fracturing fluid is described well by the lubrication equation (Batchelor, 1967). By substituting the mass conservation equation into the Navier-Stokes equations and applying the above-mentioned simplifying assumptions, the lubrication equation can be obtained:

$$\frac{\partial w(s,t)}{\partial t} = \frac{1}{12\mu}\frac{\partial}{\partial s}\left(w^3(s,t)\frac{\partial P(x,t)}{\partial s}\right), \tag{18}$$

which is true whenever Reynolds number is small i.e. laminar flow assumption (Spence and Sharp, 1985). Additionally, $w(s,t)$ is the fracture width at point s and time t, ρ is the fluid density, q is the flux per unit height and μ is the fluid viscosity.

A set of boundary conditions including a propagation criterion at the tip is required to solve the problem. The aperture of the fracture as well as the flux rate at the fracture tip is zero. If the fracture is propagation in mode I stress intensity factor K_I is equal to the fracture toughness K_{Ic}. The speed of the fluid at the front is assumed to be equal to the fracture tip speed.

The initial observation derived from equations 16-18 is that depending on the pumping rate, fracturing fluid viscosity (or generally fracturing fluid properties) and fracture height different fracture opening rate will be resulted, which means different microseismic waves will be produced.

A primary difficulty of hydraulic fracturing problems comes from the coupling of the fluid flow inside the fracture (Eq. 18) and the equation governing the rock deformations (the fracture opening which can be extracted from solution of Eq. 16). Unfortunately, analytical solutions (for instance, KGD model, Geertsma and deKlerk, 1969) are limited to fracture width at the wellbore and fracture length calculations. In general, solutions for fluid-driven fractures are tremendously difficult to construct even for simple geometries. This difficulty is due to moving boundary conditions, non-linearity of the governing equation for fluid flow in fractures, the high gradient of displacement near the fracture tip, and non-locality of the solution. Non-linearity comes from the fact that fracture permeability is a cubic function of the fracture width. Non-locality means that the fracture opening at one point is a function of fluid pressure at another point along the fracture (Detournay, 2004).

In order to address the limitations of analytical solutions for this fracture model type, and with the additional benefit of including more general geometries, we use a numerical approach to solve the above-mentioned equations. An iterative process is utilized to obtain the solution (Dahi-Taleghani and Olson, 2009). At the beginning of each time step, the net pressure distribution is assumed to be known (which is usually the net pressure distribution of the previous time step). For the first time step, a uniform net pressure distribution is assumed. The width distribution along the fracture is calculated using quadratic Extended Finite Element Methods (XFEM). In XFEM (Moës et al., 1999), discontinuities like fractures are allowed to propagate independently of the mesh configuration by permitting the discontinuity to cross the elements. Finite element space will be enriched by additional functions which have the form of analytical or asymptotic fracture solutions. The enrichment is performed from node to node in a mesh by activating extra degrees of freedom in the vicinity of the fractures. A new fluid net pressure distribution, P, is determined by solving equation (18) using the calculated width and boundary conditions. This process is repeated until reaching the convergent solution. The standard Galerkin finite element method is utilized to solve equation 18.

Results and Discussion

A comparison of Figure 5 and 6 allows us to test the numerical fracture propagation model used above (Dahi and Olson 2009) against available analytical solutions (Geertsma and de Klerk, 1969; Detournay, 2004). Figure 5 shows the expected

spectral character (frequency versus wavenumber) of far-field seismic waves emanating from a crack tip and calculated using a simple analytical approach. In Figure 6 the results are analogous except that the displacements (A) and velocities of the crack opening (B) are calculated using a numerical quasi-static approach to crack propagation. Displacements created by elastic waves radiated during incremental extension of hydraulic fractures are calculated, both ahead and vertically above the advancing fracture. Quadratic triangular elements with linear enrichment extended finite element have been used for fracture opening calculations. Displacements and velocities are estimated as a function of time and for points along the length of the crack. Both analytical and numerical approaches reveal a linear trend (~1m/s) for the higher-energy portions of the seismic data -- this slope equals the average propagation rate of the crack tip.

Table 1. Modeling parameters for hydraulic fracture pattern development

Young's modulus (**E**)	30,000 MPa
Shear modulus (μ)	12,300 MPa
Poisson's ratio (**v**)	0.22
Injection rate ($\mathbf{Q_0}$)	5 bbl/min
Fracturing Fluid viscosity	500 cP
Fracture Height (**h**)	30.33 m (100 ft)

In Figure 6A, crack opening is shown as a function of distance and time at each point along the fracture. The fracture opens in width to ~ 1cm (vertical axis) as it propagates 70 m laterally. The speed at which the crack opens along its length (Figure 6B), may be similar to that in actual hydraulic fracture tests (1 m/s) (Figure 6C) . To obtain the frequency-wave number plot to cover frequencies up to 500Hz, it is required to estimate opening profiles in 2ms time steps. In typical fracture treatments, hydraulic fracture will propagate a few millimeters in 2 ms. In order to provide adequate resolution, the element size should be ~1 mm in size, although we use linear interpolations within larger time steps (Figure 6A).

The model consists of a double-wing symmetric fracture that is aligned with the current principal in-situ stress orientations. The fracture's initial length is 5.8 meters; its center is located at the depth of 4000ft (1220 m) with 4000psi overburden stress. The minimum horizontal stress is assumed to be 90% of the maximum horizontal stress. The size of the model covers a square area, 180x180m. A non-fracture border of 10m was used to remove the edge effects. Additional modeling parameters are shown in Table 1. Since the overburden stress is the maximum principal stress fractures should remain oriented in the vertical plane. The results of this model are used in the next section to determine the frequency content of the microseism.

Spectral patterns in Figures 5 and 6 imply several expectations for real data. In the case of uneven crack velocities, the stop-and-go motion during crack propagation may change the apparent velocities revealed by the spectra. For the numerical case (Figure 6C) the central anomaly located off-origin has very low wavenumbers (~0.01/m) and frequencies which correspond to the overall shape of the velocity surface in Figure 6B. If data could be collected within the background noise at such low frequency bands in the field, spectral transforms data may be expected to reveal the size of the 'pulsating' crack. As the overall crack size grows, its spectral strength should shift toward lower frequency values.

A change in the rate of crack-tip growth should also create a change in apparent spectral velocities. Early hydraulic fracturing experiments in Los Alamos National Laboratory (Aki et al., 1982) show that the spectral peak of the continuous vibration caused by fluid injection changes with time (from 25 Hz to 15 Hz in 5 minutes) so that the dominating frequency decreases as the fracture extends by further fluid injection.

Additionally, Figure 6C spectra displays a negative velocity arm that corresponds to simultaneous growth in opposite directions of the crack. Notably, at these propagating velocities (and others we have tested up to three orders of magnitude greater), the energy concentration is always toward the lower end (< 5 Hz).

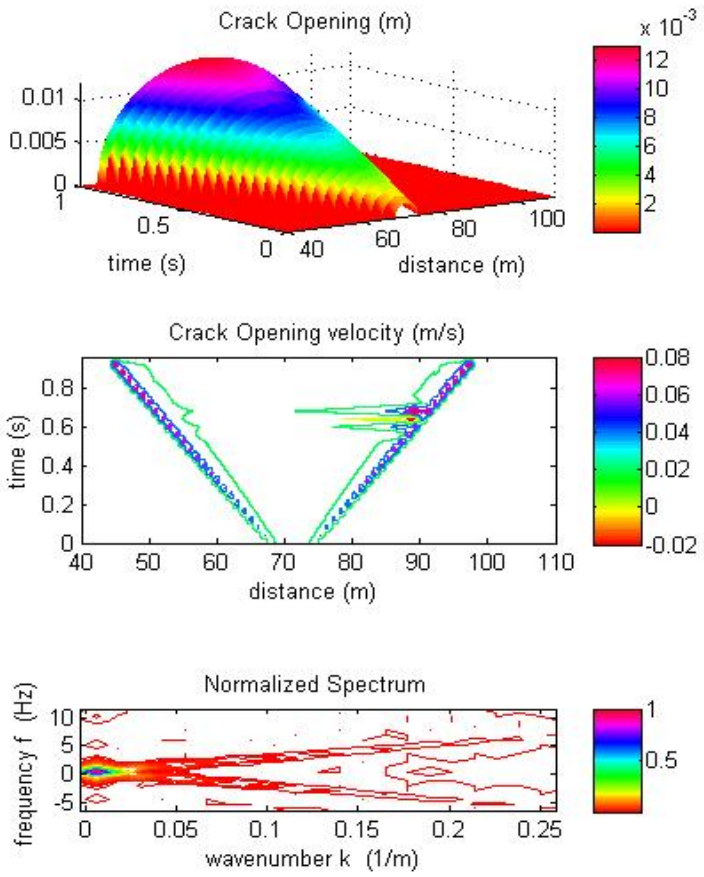

Figure 6. Display of numerical results of numerical fracture propagation model. Displacement across the opening crack (A) and its corresponding velocity field through time (B). Spectrum (frequency vs. wavenumber) of the velocity field (C) shows the relative distribution of energy across seismic arrivals in the far-field.

Band-width of the source mechanism is an important consideration for sensor selection in field monitoring of hydraulic fracturing treatments. The amplitude frequency response for ground motion for both mechanical displacement and velocity sensors goes to zero at lower frequencies (Havskov and Alguacil, 2004) and so accelerometers may be the logical choice.

Currently, common, commercial geophones (velocity sensors) start to lose their amplitude frequency response at frequencies below 4-5 Hz. Yet, sensors are relatively inexpensive, simple (requiring no external power source), and robust (in-factory calibrated for life). Short period seismometers are used extensively in local earthquake monitoring and are sensitive to 1 Hz, but are an order of magnitude larger and heavier, as well as unwieldy, require group calibration, and too fragile for use in typical seismic profiling procedures that require constant movement of the sensor array. Designs to extend the usable range of frequency of these velocity sensors (e.g., Barzilai, 2001) remain limited by these same features. Although relatively expensive, a new generation of three-component micromachined accelerometers with onboard digitization is available (Dragoset, 2005). Although these sensors provide excellent broad-band flat amplitude and linear phase response in the 1-800 MHz range (Mougenot, 2004; Pelton, 2005).

Conclusions

Herein, we try to answer basic questions regarding seismic wave emission of propagating hydraulic fractures. Our analyses were based on forward modeling. Forward problems provide insight into the mechanics of the problem. The solutions to the forward problems also provide constraint on the solution of the inverse problems, which are generally unstable (Kostrov and Das, 1989). Two different approaches are used to generate seismic source along the fractures. One solution is the analytical elastodynamics solution for fracture propagation with uniform fluid pressure, the other one is the coupled, quasi-static solution. To calculate far-field seismograms from the source, the fractures are presumed to act as a continuous distribution of

dislocations where the magnitude of dislocations is a function of fracture opening at that point. A three-dimensional elastodynamics solution for single dislocations will provide time-varying motions in the far-field due to the changes in the source.

It has been observed that microseismic sources generated by a quasi-static model and an analytical model share similar spectral characteristics. Therefore, it may not be very risky to use quasi-static models to calculate seismograms generated by hydraulic fractures. Seismic monitoring of hydraulic fracturing treatments may need to be carried record over lower frequency ranges than is typically done by industry today. The predicted range of useful frequencies suggests also use of accelerometers rather than velocity geophones. As more data from industry becomes available for examination we expect that these questions may be better addressed. Results from the study of natural hydraulic fracture processes suggest that mining current microseismic monitoring data for lower-frequency events could reveal true tensile events.

Nomenclature

μ …… shear modulus
ν ….... Poisson's ratio
ρ …… density
ω …… frequency
a …… fracture half-length
C ….. Elasticity tensor
E ….. Young's modulus of elasticity
h …… fracture height
M ….. moment tensor
P …… net pressure
Q_0 …. fluid injection rate
r …… the distance between seismic source and receiver
t …… time
u ….. displacement
v ….. fracture propagation speed
V_P …. rock compressional wave velocity
V_S …. rock shear wave velocity
V ….. wave propagation speed
w ….. fracture width
x_i ….. i-th component of the position vector

REFERENCES

Adachi, J., Siebrits, E., Peirce, A., and Desroches, J., 2007, Computer simulation of hydraulic fractures: International Journal of Rock Mechanics and Mining Sciences, v. 44, p. 739-757.

Aki, K., Fehler, M., Aamodt, R.L., Albright, J.N., Potter, R.M., Pearson, C.M., and Tester, J.W., 1982, Interpretation of Seismic Data From Hydraulic Fracturing Experiments at the Fenton Hill, New Mexico, Hot Dry Rock Geothermal Site: J. Geophys. Res., v. 87, p. 936-944.

Aki, K., Fehler, M., and Das, S., 1977, Volume 2: Netherlands, Elsevier: Amsterdam, Netherlands, p. 259-287.

Bame, D., and Fehler, M., 1986, Observations of long period earthquakes accompanying hydraulic fracturing: Geophys. Res. Lett., v. 13, p. 149-152.

Barzilai, A.M., 2001, An affordable, broadband seismometer; improving the low frequency performance of geophones: United States.

Boone, T.J., and Ingraffea, A.R., 1990, A numerical procedure for simulation of hydraulically-driven fracture propagation in poroelastic media: International Journal for Numerical and Analytical Methods in Geomechanics, v. 14, p. 27-47.

Broberg, K.B., 1975, On stable crack growth: Journal of the Mechanics and Physics of Solids, v. 23, p. 215-237.

Burridge, R., and Knopoff, L., 1964, Body force equivalents for seismic dislocations: Bulletin of the Seismological Society of America, v. 54, p. 1875-1888.

Chouet, B.A., 1996, Long-period volcano seismicity: its source and use in eruption forecasting: Nature, v. 380, p. 309-316.

Dahi-Taleghani, A., and Olson, J.E., 2009, Analysis of multi-stranded hydraulic fracture Propagation: an improved model for the interaction between induced and natural fractures, SPE ATCE New Orleans, LA, SPE 124884.

Dahi Taleghani, A., 2009, Analysis of Hydraulic Fracture Propagation in Fractured Reservoirs: an improved model for the interaction between induced and natural fractures, PhD dissertation, The university of Texas at Austin.

Detournay, E., 2004, Propagation Regimes of Fluid-Driven Fractures in Impermeable Rocks: International Journal of Geomechanics, v. 4, p. 35-45.

Dragoset, B., 2005, Expert answers: Digital geophones: The Leading Edge, v. 24, p. 131-135.

Dreger, D.S., 2000, Dilational processes accompanying earthquakes in the Long Valley Caldera: Science, v. 288, p. 122-125.
Eisner, L., Duncan, P.M., Heigl, W.M., and Keller, W.R., 2009, Uncertainties in passive seismic monitoring: The leading Edge, v. 28, p. 648-655.
Ford, S.R., 2009, Identifying isotropic events using a regional moment tensor inversion: Journal of Geophysical Research, v. 114.
Freund, L.B., 1990, Dynamic Fracture Mechanics, Cambridge University Press, 584 p.
Geertsma, J., de Klerk, F., 1969, A rapid method of predicting width and extent of hydraulically induced fractures, Journal of Petroleum Technology, Vol. 21, pages: 1571–81 [SPE 2458].
Havskov, J., and Alguacil, G., 2004, Instrumentation in Earthquake Seismology, Springer, 358 p.
Kostrov, B.V., and Das, S., 1989, Principles of Earthquake Source Mechanics Cambridge University p. 308.
McNutt, S.R., 2005, Volcanic Seismology: Annual Review of Earth & Planetary Sciences, v. 33, p. 461-C-3.
Moës, N., Dolbow, J. and T. Belytschko, 1999, A finite element method for crack growth without remeshing, International Journal for Numerical Methods in Engineering, Volume 46, Pages 131-150.
Mougenot, D., 2004, How digital sensors compare to geophones, SEG Annual Meeting, Volume 75: Expanded Abstracts, p. 5-8.
Ouyang, S., Carey, G.F., and Yew, C.H., 1997, An Adaptive Finite Element Scheme for Hydraulic Fracturing with Proppant Transport: International Journal for Numerical Methods in Fluids, v. 24, p. 645-670.
Pelton, J., 2005, Near-surface seismology: Surface based methods, *in* Butler, D.K., ed., Near Surface Geophysics, Volume 13: Investigations in Geophysics: Tulsa, Society of Exploration Geophysicists, p. 219-263.
Rice, J. R., 1980, Elastic Wave Emission from Damage Processes, Journal of Nondestructive Evaluation, 1, 1980, pp. 215-224.
Rice, J.R., 1980b, The Mechanics of Earthquake Rupture, Physics of the Earth's Interior (Proc. International School of Physics 'Enrico Fermi', Course 78, 1979; ed. A. M. Dziewonski and E. Boschi), Italian Physical Society and North-Holland Publ. Co., pp. 555-649.
Shi, Z. and Y. Ben-Zion, 2009, Seismic radiation from tensile and shear point dislocations between similar and dissimilar solids. Geophysical Journal International, Vol. 179, pp. 444–458.
Spence, D.A., and Sharp, P., 1985, Self-Similar Solutions for Elastohydrodynamic Cavity Flow: Proceedings of the Royal Society of London. Series A, Mathematical and Physical Sciences, v. 400, p. 289-313.
Vidale, J.E., Goes, S., and Richards, P.G., 1995, Near-field deformation seen on distant broadband seismograms: Geophysical Research Letters, v. 22, p. 1-4.